Two Co(II) Complexes Constructed from 1-(3,5-Dicarboxybenzyl)-3,5-pyrazole Dicarboxylic Acid: Syntheses, Structures and Magnetic Properties①

WANG Lao-Bang WANG Ji-Jiang② TANG Long②
WANG Xiao HOU Xiang-Yang
YUE Er-Lin ZHANG Yu-Qi
(*Yan'an City Key Laboratory of New Energy & New Functional Materials, Shaanxi Key Laboratory of Chemical Reaction Engineering, College of Chemistry and Chemical Engineering, Yan'an University, Yan'an* 716000, *China*)

ABSTRACT Two new complexes $[Co_2(L)(4,4'\text{-bip})(H_2O)_3]_n$ (**1**) and $\{[Co(L')_2(phen)]\cdot 2H_2O)\}_n$ (**2**) (H_4L = 1-(3,5-dicarboxybenzyl)-3,5-pyrazole dicarboxylic acid, H_3L' = 1-(3,5-dicarboxybenzyl)-3-pyrazole carboxylic acid, 4,4′-bip = 4,4′-bis(1-imidazolyl)biphenyl, phen = 1,10-phenanthroline) were synthesized. Complexes **1** and **2** have been characterized by IR spectrography, X-ray single-crystal diffraction, elemental analysis and thermogravimetry. **1** crystallizes in monoclinic system, space group $P2_1/c$. Complex **2** crystallizes in monoclinic system, space group $I2/a$. It is remarkable that *in situ* hydrothermal decarboxylation was observed during preparing complex **2**. In addition, magnetic analysis indicates that antiferromagnetic interaction exists among Co(II) ions in complexes **1** and **2**.

Keywords: Co(II), 1-(3,5-dicarboxybenzyl)-3,5-pyrazole dicarboxylic acid, magnetic properties;
DOI: 10.14102/j.cnki.0254–5861.2011–3071

1 INTRODUCTION

With the development of chemistry[1-3], coordination polymers (CPs) due to their charming structures and wide applications in proton conduction[4], magnetism[5], conductivity[6], heterogeneous catalysis[7], gas storage and separation[8, 9] and luminescence detection have attracted more attention[10, 11]. For coordination polymers, metal ions and organic components play an essential role. As is well known, the construction of CPs can be affected by the flexibility of ligand. Pyrazole carboxylic acids are widely investigated and result in a large number of coordination polymers due to diverse coordination modes[12]. The pyrazole carboxylic acid ligands can satisfy the coordination number of metal atoms (such as Co and Zn) using the synthesis of different dimensions of CP. Because pyrazole carboxylic acids can provide sufficient oxygen and nitrogen atoms[13] and cobalt atoms have a variety of coordination modes, they are easy to form stable complexes.

In this background, we synthesized two new complexes by using 1-(3,5-dicarboxybenzyl)-3,5-pyrazole dicarboxylic acid. In addition, thermal and magnetic analyses of complexes **1** and **2** have also been investigated. During the synthesis of **2**, the H_4L ligand was decarboxylated *in situ* to form H_3L' (Scheme 1). We suggest that the synergetic effects of both phen and Co(II) ions are important factors in controlling the formation of H_3L' ligand[14]. Generally, under hydrothermal conditions, some ligands can easily lose partial carboxyl group, which can be proceeded by the cleavage of unstrained C–C bond, and then construct lots of unpredictable complexes. Many reports indicate that metal ions, reaction temperature and pH value play unique catalytic roles in the decarboxylation reaction[15, 16].

Received 17 December 2020; accepted 10 March 2021 (**CCDC 2047953 and 2047954**)
① This work was supported by the National Natural Science Foundation of China (No. 21373178)
② Corresponding authors. Wang Ji-Jiang (1973-), professor, majoring in functional coordination chemistry. E-mail: yadxwjj@126.com
Tang Long (1976-), associate professor, majoring in functional coordination chemistry. E-mail: ydtanglong@163.com

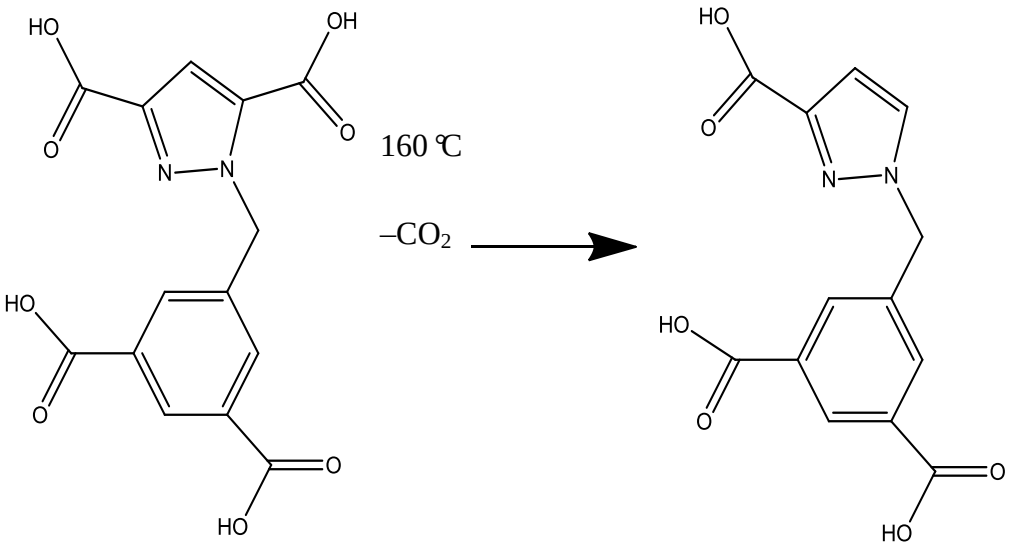

Scheme 1. Hydrothermal decarboxylation of H_4L

2 EXPERIMENTAL

2. 1 Materials and methods

All reagents and solvents in the present work were obtained from commercial sources and used without further purification. Elemental analyses for C, H and N were collected on a PerkinElmer PE-2400 elemental analyzer. The FT-IR spectrum was measured using KBr pellets with a Nicolet 170SX FT-IR spectrophotometer in the range of 4000～400 cm^{-1}. The magnetic susceptibility data were investigated by using Quantum Design MPMS SQUID VSM instrument in the range of 2～300 K.

2. 2 Synthesis

2. 2. 1 $[Co_2(L)(4,4'\text{-bip})(H_2O)_3]_n$ (1)

A mixture of $Co(NO_3)_2 \cdot 6H_2O$ (0.10 mmol, 29.1 mg), 4,4′-bip (0.05 mmol, 14.3 mg) and H_4L (0.05 mmol, 16.7 mg) in 15 mL H_2O was placed in a 25 mL Teflon-lined autoclave and the temperature was increased from room temperature to 160 ℃ within 2 h, heated to 160 ℃ for 3 days, and then cooled to room temperature at a rate of 10 ℃·h^{-1}. Purple crystals of complex **1** were obtained (yield: 46% based on 4,4′-bip). Anal. Calcd. for $C_{32}H_{26}N_6O_{11}Co_2$: C, 48.70; H, 3.30; N, 10.65%. Found: C, 48.69; H, 3.28; N, 10.59%. IR (KBr, cm^{-1}): 3420 (w), 2364 (w), 2343 (w), 1618 (s), 1542 (s), 1345 (s), 1309 (w), 1124 (m), 1066 (w), 647 (w).

2. 2. 2 $\{[Co(L')_2(phen)]\cdot 2H_2O\}_n$ (2)

A mixture of $Co(NO_3)_2 \cdot 6H_2O$ (0.30 mmol, 87.3 mg), phen (0.6 mmol, 118.9 mg) and H_4L (0.6 mmol, 100.2 mg) in 15 mL H_2O was placed in a 25 mL Teflon-lined autoclave and the temperature was raised from room temperature to 160 ℃ within 2 h, heated to 160 ℃ for 3 days, and cooled to room temperature at a rate of 10 ℃·h^{-1}. Purple crystals of complex **2** were obtained (yield: 72% based on H_4L). Anal. calcd. for $C_{38}H_{30}N_6O_{14}Co$: C, 53.42; H, 3.51; N, 9.84%. Found: C, 53.43; H, 3.47; N, 9.86%. IR (KBr, cm^{-1}): 3482 (w), 2963 (w), 2600 (w), 2367 (w), 1705 (s), 1609 (s), 1508 (m), 1425 (s), 1366 (m), 1298 (m), 1202 (w), 1080 (w), 849 (m), 768 (m), 729 (w), 673 (w), 636 (w).

2. 3 Crystal structure determination

Crystal data for **1** and **2** were collected on a Bruker Smart APEX II CCD diffractometer using Mo*Kα* radiation (λ = 0.71073 Å) in an ω-scan mode. A semiempirical absorption correction was applied with the SADABS program. By using the SHELXL 2014 programs, the structure was solved by direct methods and refined by full-matrix least-squares on F^2[17, 18]. All non-hydrogen atoms were refined anisotropically and all hydrogen atoms were geometrically placed in the calculated positions. The detailed crystallographic data are presented in Table 1. Selected bond lengths and bond angles are listed in Table 2.

Table 1. Crystal Data and Structure Refinement for Complexes 1 and 2

Complex	**1**	**2**
Empirical formula	$C_{32}H_{26}Co_2N_6O_{11}$	$C_{38}H_{30}CoN_6O_{14}$
Formula weight	788.45	853.61
Crystal system	Monoclinic	Monoclinic
Space group	$P2_1/c$	$I2/a$
Temperature/K	296(2)	296(2)
Wavelength/Å	0.71073	0.71073
a/Å	15.759(5)	11.455(3)
b/Å	13.789(5)	20.722(6)
c/Å	15.370(5)	16.546(4)
α/°	90	90
β/°	105.306(5)	109.915(15)
γ/°	90	90
V/Å^3	3221.4(18)	3692.7(17)
Z	4	4
D_c (g cm^{-3})	1.626	1.535
μ/mm^{-1}	1.103	0.546
F(000)	1608	1756
θ range/°	1.994 to 30.960	2.619 to 28.232
Limiting indices	$-22\leqslant h\leqslant 11$, $-15\leqslant k\leqslant 19$, $-19\leqslant l\leqslant 19$	$-15\leqslant h\leqslant 9$, $-25\leqslant k\leqslant 27$, $-18\leqslant l\leqslant 22$
No. of reflections collected	20916	11241
No. of unique rflns.	8563	4459
No. of parameters	472	275
Goodness of fit on F^2	0.957	0.975
Final R, indices ($I > 2\sigma(I)$)	R = 0.0424, wR = 0.1265	R = 0.0513, wR = 0.1217
R indices (all data)	R = 0.0620, wR = 0.1408	R = 0.0836, wR = 0.1387
Largest diff. peak, and hole (e·Å^{-3})	1.636 and –0.449	0.688 and –0.504

Table 2. Selected Bond Lengths (Å) and Bond Angles (°) for 1 and 2

Complex **1**

Bond	Dist.	Bond	Dist.	Bond	Dist.
Co(1)–N(5)	2.110(2)	Co(1)–O(2)	2.1340(18)	Co(1)–O(11)	2.1685(19)
Co(1)–N(1)	2.223(2)	Co(1)–O(3B)	2.0400(19)	Co(1)–O(8C)	2.0761(18)
Co(2)–O(6A)	2.0380(19)	Co(2)–N(3)	2.082(2)	Co(2)–O(10)	2.103(2)
Co(2)–O(9)	2.137(2)	Co(2)–O(1)	2.163(2)	Co(2)–O(2)	2.2807(18)
Angle	(°)	Angle	(°)	Angle	(°)
O(3B)–Co(1)–O(8C)	85.46(8)	O(3B)–Co(1)–N(5)	94.88(9)	O(8C)–Co(1)–N(5)	91.93(8)
O(3B)–Co(1)–O(2)	98.84(8)	O(8C)–Co(1)–O(2)	172.52(7)	N(5)–Co(1)–O(2)	93.78(8)
O(3B)–Co(1)–O(11)	174.16(8)	O(8C)–Co(1)–O(11)	88.73(7)	N(5)–Co(1)–O(11)	85.99(8)
O(6A)–Co(2)–N(3)	99.76(9)	O(6A)–Co(2)–O(10)	84.81(8)	N(3)–Co(2)–O(10)	96.27(11)
O(6A)–Co(2)–O(9)	91.70(8)	N(3)–Co(2)–O(9)	87.09(9)	O (10)–Co(2)–O(9)	175.51(9)
O(6A)–Co(2)–O(1)	106.54(8)	N(3)–Co(2)–O(1)	152.86(9)	O(10)–Co(2)–O(1)	92.72(10)

Symmetry codes: A $-x+1, -y, -z$; B $-x+1, y+1/2, -z+1/2$; C $-x+1, -y, -z+1$

Complex **2**

Bond	Dist.	Bond	Dist.	Bond	Dist.
Co(1)–O(1)	2.1229(17)	Co(1)–O(1A)	2.1230(17)	Co(1)–N(3A)	2.153(2)
Co(1)–N(3)	2.153(2)	Co(1)–N(1)	2.156(2)	Co(1)–N(1A)	2.156(2)
Angle	(°)	Angle	(°)	Angle	(°)
O(1)–Co(1)–O(1A)	101.77(10)	O(1)–Co(1)–N(3A)	90.87(8)	O(1A)–Co(1)–N(3A)	166.62(7)
O(1)–Co(1)–N(3)	166.62(7)	O(1A)–Co(1)–N(3)	90.87(8)	N(3A)–Co(1)–N(3)	76.91(11)
O(1)–Co(1)–N(1)	77.13(7)	O(1A)–Co(1)–N(1)	85.85(8)	N(3A)–Co(1)–N(1)	101.41(8)

Symmetry code: A $-x+3/2, y, -z+1$

3 RESULTS AND DISCUSSION

3. 1 Crystal structure of $[Co_2(L)(4,4'\text{-bip})(H_2O)_3]_n$ (1)

The result of X-ray single-crystal diffraction analysis reveals that complex **1** crystallizes in monoclinic $P2_1/c$ space group. The asymmetric unit consists of two Co(II) ions, one H_4L ligand, one 4,4′-bip ligand and three coordination water molecules. As shown in Fig. 1a, Co(1) and Co(2) are both six-coordinated in different coordination environments. Co(1) is surrounded by O(2), O(3B) and O(8C) from three H_4L ligands, N(1) from one H_4L ligand, O(11) from one coordination water molecule, and N(5) from one 4,4′-bip. While Co(2) is coordinated by O(1), O(2), O(6A) from two H_4L ligands, N(3) from one 4,4′-bip ligand, and O(9), O(10) from two coordination water molecules. The Co–O bond lengths vary from 2.0380(19) to 2.2807(18) Å, and the Co–N distances are within the range of 2.082(2)～2.223(2) Å (Table 2).

As shown in Fig. 1c, Co(II) ions are connected to L^{4-} to form a 1D chain. The 1D chain forms a 2D planar structure through the connection of Co(II) ions (Fig. 1c) viewed from the *b* direction. Interestingly, this structure along the *b* direction is connected to form a 3D structure through 4,4′-bip (Fig. 1d).

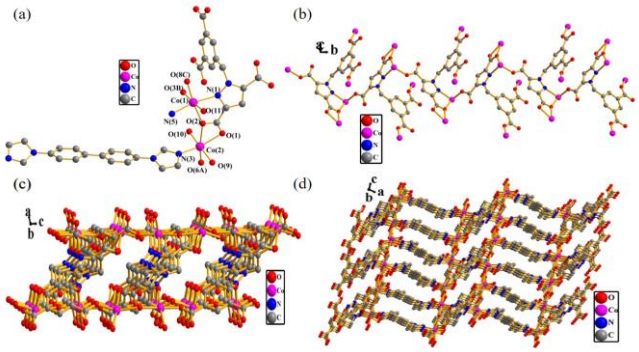

Fig. 1. (a) Coordination environment of the Co(II) in 1. Symmetry codes: A: –*x*+1, –*y*, –*z*; B: –*x*+1, *y*+1/2, –*z*+1/2; C: –*x*+1, –*y*, –*z*+1. (b) 1D chain structure of 1. (c) 2D framework of 1. (d) 3D framework of 1

3. 2 Crystal structure of $\{[Co(L')_2(phen)]\cdot 2H_2O\}_n$ (2)

The result of X-ray single-crystal diffraction analysis reveals that complex **2** crystallizes in the monoclinic *I2/a* space group. The asymmetric unit consists of one Co(II) ion, two L^{3-} ions, one phen ligand and two free water molecules. Co(II) in the molecule adopts a 6 coordination mode, forming a twisted octahedral coordination configuration. As show in Fig. 2a, Co(II) is surrounded by O(1), O(1A) from two different L^{3-} ions, N(3), N(3A) from one phen ligand, and N(1), N(1A) from two different L^{3-} ions. The Co–O bond lengths vary from 2.1229(17) to 2.1230(17) Å, and the Co–N distances are within the range of 2.153(2)～2.156(2) Å (Table 2).

The molecules of complex **2** form a one-dimensional chain structure through the hydrogen bonding of O(7)–H(7A)··O(2E), O(7)–H(7B)··O(1F), O(4)–H(4)··O(7C) and O(5)–H(5)··O(2D), O(7C) from free water molecules, and O(1F), O(2E), and O(4) from L^{3-} ions (Fig. 2c). The detailed information of hydrogen bond is shown in Table 3. The 3D supramolecular structure is shown in Fig. 2c viewed from the *a* direction.

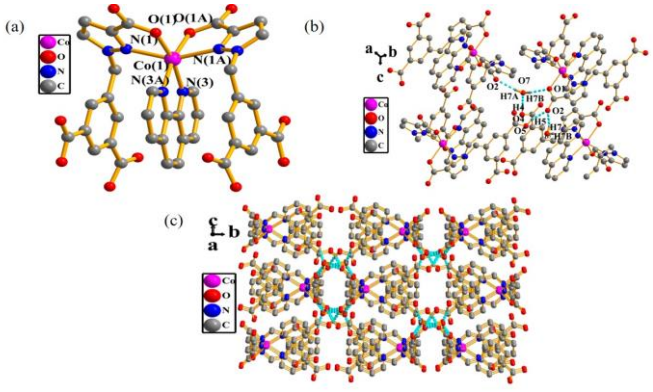

Fig. 2. (a) Coordination environment of the Co(II) in 2. Symmetry codes: A: –*x*+3/2, *y*, –*z*+1.

(b) 1D chain structure of 2. (c) 3D supramolecular framework of 2

Table 3. Hydrogen Bond Lengths (Å) and Bond Angles (°) for Complex 2

D–H ··A	d(D–H)	d(H ··A)	d(D–A)	∠DHA
O(4)–H(4) ··O(7C)	0.82	1.84	2.658(3)	172
O(5)–H(5) ··O(2D)	0.82	1.86	2.630(3)	155
O(7)–H(7A) ··O(2E)	0.85(3)	2.11(3)	2.927(3)	160(3)
O(7)–H(7B) ··O(1F)	0.86(2)	2.06(3)	2.878(3)	161(3)

Symmetry codes: C: –1/2+*x*, –1/2+*y*, –1/2+*z*; D: –1+*x*, –1/2–*y*, –1/2+*z*; E: –1+*x*, –1+*y*, –1+*z*; F: –3/2+*x*, –*y*, –1+*z*

3. 3 Thermal analysis

To explore the stabilities of complexes **1** and **2**, their thermogravimetric analyses (TGA) were carried out under a nitrogen atmosphere from room temperature to 900 ℃ (Fig. 3). In **1**, the first weight loss of 6.50% is in the range from 25 to 260 ℃ corresponding to the removal of three coordinated H_2O (calcd. 6.85%). When further heated to about 300 ℃, the 3D framework begins to decompose. In complex **2**, the first weight loss of 4.63% is in the range from 25 to 330 ℃ due to the removal of two free water molecules (calcd. 4.21%). When continuing heating to about 350 ℃, the 3D supramolecular framework begins to decompose.

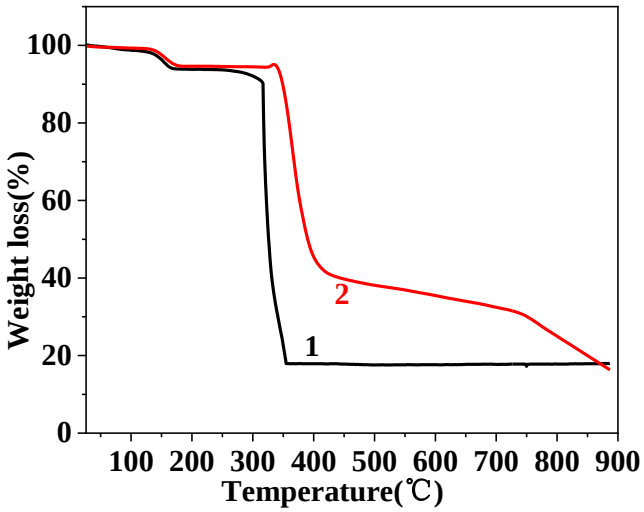

Fig. 3. Thermogravimetric analyses for 1 and 2

Powder X-ray diffraction (PXRD) testing was performed to prove the phase purity of the two complexes. The simulated and experimental peaks of **1** and **2** basically coincide (Fig. 4), indicating that the purity of the sample was good.

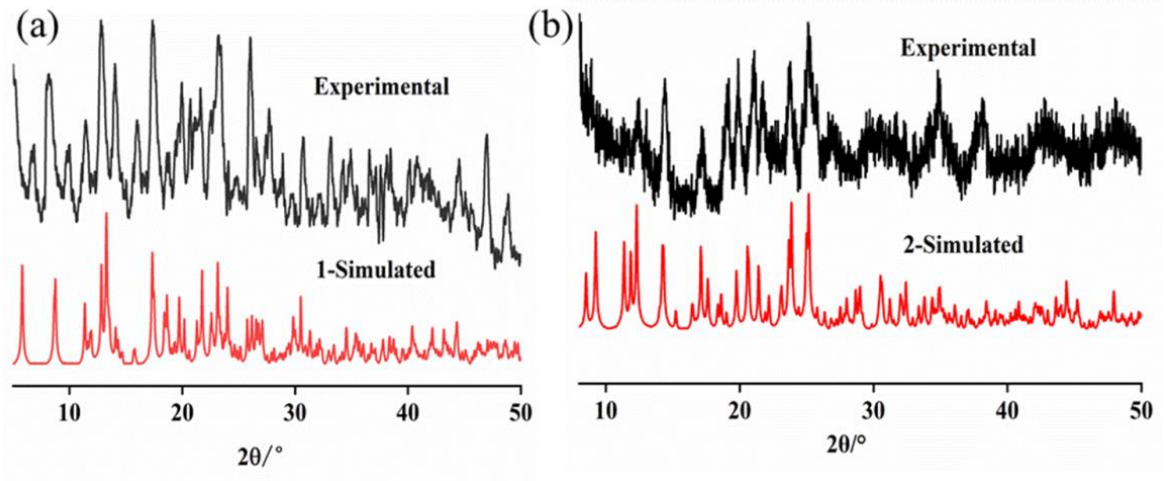

Fig. 4. PXRD of 1 and 2

3. 4 Magnetic properties

The magnetic properties of **1** and **2** were measured in a range of 2～300 K at 1000 Oe. The magnetic susceptibility data for **1** are shown in Fig. 5. As observed, the experimental $\chi_M T$ value was 3.456 $cm^3 \cdot K \cdot mol^{-1}$ at 300 K, which is lower than the theoretical value (3.75 $cm^3 \cdot K \cdot mol^{-1}$) of two isolated spin-only Co(II) ions (S = 3/2). As the temperature gradually decreased, the value of $\chi_M T$ decreased slowly and the value of $\chi_M T$ decreased to 0.411 $cm^3 \cdot K \cdot mol^{-1}$. When at 2 K, antiferromagnetic interactions are operative. The magnetic susceptibility *vs.* T of **1** followed the $H = -2JS_{Co1}S_{Co2}$, and the magnetic susceptibility expression for a dinuclear models is given by[19]:

$$\chi_M = \frac{2Ng^2\beta^2}{kT} \frac{e^{2J/(kT)} + 5e^{6J/(kT)} + 14e^{12J/(kT)}}{1 + 3e^{2J/(kT)} + 5e^{6J/(kT)} + 7e^{12J/(kT)}}$$

The least-squares fit to the experimental data was carried out with g = 2.10, J = –0.454 cm^{-1} and $R = 5.249 \times 10^{-3}$. The negative value of J in complex **1** further reveals that the antiferromagnetic interaction exists among the Co(II) ion centers.

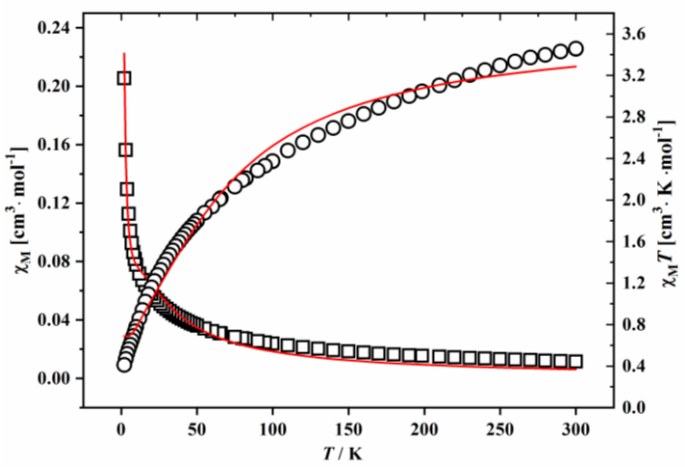

Fig. 5. Thermal variation of χ_M and $\chi_M T$ for 1 (Open points are the experimental data, and the solid line represents the best fit obtained from the Hamiltonian given in the text)

The magnetic susceptibility data measured for **2** are shown in Fig. 6. As observed, the experimental $\chi_M T$ value was 3.294 $cm^3 \cdot K \cdot mol^{-1}$ at 300 K, which is lower than the theoretical one (3.75 $cm^3 \cdot K \cdot mol^{-1}$) of two isolated spin-only Co(II) ions (S = 3/2). As the temperature gradually decreased, the value of $\chi_M T$ decreased slowly and that of $\chi_M T$ decreased to 2.032 $cm^3 \cdot K \cdot mol^{-1}$. At 2 K, the antiferromagnetic interactions are operative. The magnetic susceptibility *vs.* T of **2** followed $H = -2JS$. The least-squares fit to the experimental data was carried out with g = 2.05, J = –0.255 cm^{-1} and $R = 1.05 \times 10^{-3}$. The negative value of J in **2** further reveals antiferromagnetic interaction existing among the Co(II) ion centers.

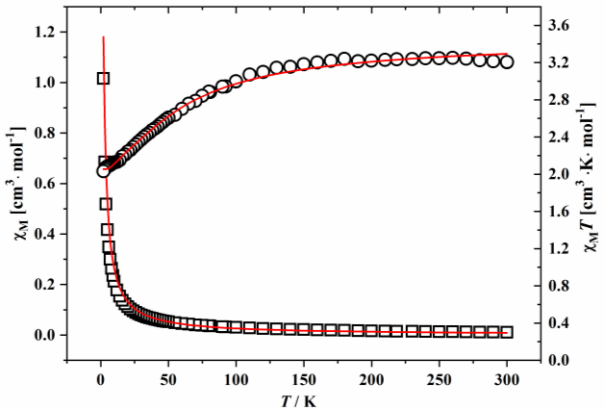

Fig. 6. Thermal variation of χ_M and $\chi_M T$ for 2

4 CONCLUSION

In summary, two new cobalt complexes were successfully synthesized by using 1-(3,5-dicarboxybenzyl)-3,5-pyrazole dicarboxylic acid as a ligand under hydrothermal conditions. The structural studies reveal that complexes **1** and **2** show 3D frameworks. Besides, magnetic analysis indicates antiferromagnetic interaction existing among the Co(II) ion centers in **1** and **2**.

REFERENCES

（1） Rouffet, M.; de Oliveira, C. A. F.; Udi, Y.; Agrawal, A.; Sagi, I.; McCammon, J. A.; Cohen, S. M. From sensors to silencers: quinoline- and benzimidazole-sulfonamides as inhibitors for zinc proteases. *J. Am. Chem. Soc*. **2010**, 132, 8232–8233.

（2） Liu, H. Y.; Wu, H.; Ma, J. F.; Liu, Y. Y.; Liu, B.; Yang, J. Syntheses, structures, and photoluminescence of zinc(II) coordination polymers based on carboxylates and flexible bis-[(pyridyl)-benzimidazole] ligands. *Cryst. Growth Des*. **2010**, 10, 4795–4805.

（3） Xue, F.; Kumar, P.; Xu, W. Q.; Mkhoyan, K. A.; Tsapatsis, M. Direct synthesis of 7 nm-thick zinc(II)-benzimidazole-acetate metal-organic framework nanosheets. *Chem. Mater*. **2018**, 30, 69–73.

（4） Yang, F.; Xu, G.; Dou, Y. B.; Wang, B.; Zhang, H.; Wu, H.; Zhou, W.; Li, J. R.; Chen, B. L. A flexible metal-organic framework with a high density of sulfonic acid sites for proton conduction. *Nat. Energy* **2017**, 2, 877−883.

（5） Wang, Y. L.; Han, C. B.; Zhang, Y. Q.; Liu, Q. Y.; Liu, C. M.; Yin, S. G. Fine-tuning ligand to modulate the magnetic anisotropy in a carboxylate-bridged Dy2 single-molecule magnets system. *Inorg. Chem.* **2016**, 55, 5578–5584.

（6） Horike, S.; Umeyama, D.; Kitagawa, S. Ion conductivity and transport by porous coordination polymers and metal-organic frameworks. \ *Chem. Res*. **2013**, 46, 2376–2384.

（7） Zhao, M.; Ou, S.; Wu, C. D. Porous metal-organic frameworks for heterogeneous biomimetic catalysis. *Chem. Res*. **2014**, 47, 1199–1207.

（8） Kitagawa, S.; Kitaura, R.; Noro, R. Functional porous coordination polymers. *Angew. Chem. Int. Ed.* **2004**, 43, 2334–2375.

（9） He, Y. B.; Zhou, W.; Qian, G. D.; Chen, B. L. Methane storage in metal-organic frameworks. *Chem. Soc. Rev*. **2014**, 43, 5657−5678.

(10) Lustig, W. P.; Mukherjee, S.; Rudd, N. D.; Desai, A. V.; Li, J.; Ghosh, S. K. Metal-organic frameworks: functional luminescent and photonic materials for sensing applications. *Chem. Soc. Rev*. **2017**, 46, 3242–3285.

(11) Lin, Z. T.; Wang, Y. L.; Liu, Q. Y. Crystal structure and luminescence of a Cd(II) complex based on the 3,3′,5,5′-tetrafluorobiphenyl-4,4′-dicarboxylate and adenine ligands. *Chin. J. Struct. Chem.* **2020**, 11, 2041−2045.

(12) Zhang, N.; Guo, Y. H.; Yu, Y. Z.; Wang, Z.; Niu, Y. S.; Wu, X. L. Solvothermal synthesis, crystal Structure and luminescence property of a 1D silver(I) coordination polymer. *Chin. J. Struct. Chem.* **2020**, 11, 2009−2015.

(13) Verma, P.; Singh, U. P.; Butcher, R. Luminescent metal organic frameworks for sensing and gas adsorption studies. *CrystEngComm*. **2019**, 21, 5470–5481.

(14) Wang, J. J.; Cao, Z.; Wang, X.; Tang, L.; Hou, X. Y.; Ju, P.; Ren, Y. X.; Chen, X. L.; Zhang, Y. Q. A novel 3D Cd(II) coordination polymer generated *via in situ* ligand synthesis involving C–O esterbond formation. *RSC Adv.* **2019**, 9, 307–312

(15) Liu, C. B.; Li, Q.; Wang, X.; Che, G. B.; Zhang, X. J. A series of lanthanide(III) coordination polymers derived via in situ hydrothermal decarboxylation of quinoline-2,3-dicarboxylic acid. *Inorg. Chem. Commun*. **2014**, 39, 56–60.

(16) Yang, A. H.; Zou, J. Y.; Wang, W. M.; Shi, X. Y.; Gao, H. L.; Cui, J. Z.; Zhao, B. Two three-dimensional lanthanide frameworks exhibiting luminescence increases upon dehydration and novel water layer involving in situ decarboxylation. *Inorg. Chem.* **2014**, 53, 7092–7100.

(17) Sheldrick, G. M. SHELXS-2014/7 and SHELXL-2014/7 program for solution and refinement of crystal structures. *Institute for Inorganic Chemistry*. University of Göttingen, Göttingen, Germany **2014**.

(18) Sheldrick, G. M. Crystal structure refinement with SHELXL. *Acta Cryst*. **2015**, C71, 3–8.

(19) Ishida, T.; Kawakami, T.; Mitsubori, S.; Nogami, T.; Yamaguchi, K.; Iwamura, H. Antiferromagnetic coupling of transition metal spins across pyrimidine and pyrazine bridges in dinuclear manganese(II), cobalt(II), nickel(II) and copper(II) 1,1,1,5,5,5-hexafluoropentane-2,4-dionate complexes. *J. Chem. Soc. Dalton Trans.* **2002**, 3177–3186.